2

A Practical Demonstration of Spectrum Sensing for WiMAX Based on Cyclostationary Features

Gianmarco Baldini[1], Raimondo Giuliani[1], Diego Capriglione[1]
and Kandeepan Sithamparanathan[2]
[1]*Joint Research Centre - European Commission*
[2]*RMIT University*
[1]*Italy*
[2]*Australia*

1. Introduction

Wireless communication systems rely on the use of radio frequency spectrum. The advent of new wireless applications and services and the increasing demand for higher data rates and broadband wireless connectivity have worsen the problem of "'spectrum scarcity"'. It is more and more difficult for spectrum regulators to identify new spectrum bands for new wireless services, because the existing radio frequency spectrum is already allocated to the licensed services. This is also a consequence of the traditional spectrum licensing scheme, where spectrum bands are statically allocated to wireless services in a specific region.

At the same time, recent studies have shown that the spectrum bands are significantly underutilized in time or space. The FCC Spectrum Policy Task Force has reported in (FCC, 2002) vast temporal and geographic variations in the usage of allocated spectrum with utilization ranging from 15% to 85%. Cognitive Radio (CR) technology ((Mitola, 1999), (Haykin, 2007) and (Bhargava, 2007)) offers an alternative to the current system of static spectrum allocation policy by allowing an unlicensed user to share the same radio spectrum resources with the primary user.

To perform the sharing of spectrum resources, CR devices must be able to sense the environment over huge swaths of spectrum to detect spectral holes and to expediently use frequency bands that are not used by primary users, without causing harmful interference to legacy systems. A potential application for CR technology is the "'White Spaces"'concept. The CR nodes opportunistically utilize the spectrum as a secondary user by identifying the 'gaps' in the spectrum known as the 'white space'. The white space arises from partial occupancies of the incumbent users of the spectrum known as the primary users (PU) (e.g. Digital TV broadcasters). The secondary communication by the CR can be performed as long as the white spaces are identified in the spatio-temporal domain (FCC, 2010). The radio spectrum regulatory bodies around the world have also shown great interest in CR technology to improve spectrum utilization (FCC, 2003), (EC, 2007), but the risk of wireless interference to licensed users remains an important concern.

One of the key challenges of CR technology is to reliably detect the presence or absence of primary users at very low signal-to-noise ratio. There are various spectrum sensing

techniques available such as the energy detector based sensing, waveform-based sensing, cyclostationarity-based sensing and others (Arslan, 2009). The energy detection method performs the signal measurements and determines the unoccupied spectrum bands by comparing the estimated power to predetermined threshold values. However this method does not perform well under low signal-to-noise ratio conditions.

In this paper we adopt the cyclostationarity-based sensing by considering practical demonstrations and experimentations. Wireless transmissions in general show very strong cyclostationarity features depending on their modulation type, data rate and carrier frequency etc., especially when excess bandwidth is utilized. Therefore the identification of the unique set of features of a particular radio signal for a given wireless access system can be used to detect the system based on its cyclostationarity features. Spectrum sensing based on cyclostationarity performs very well with very low signal-to-noise ratio as described in (Cabric, 2007), (Jondral, 2004).

Spectrum sensing based on cyclostationarity features has received considerable attention from the academic community from the initial papers by Gardner (Gardner, 1991) and (Gardner, 1975), which highlighted that most of the communication signals can be modeled as cyclostationary that exhibits underlying periodicities in their signal structures.

Cyclostationary spectrum sensing has been investigated in (Hosseini, 2010) which addresses the problem that in many applications, for a specific signal, the statistical characteristics are not the same in two adjacent periods, but they change smoothly. So, the periodicity which appears in the aforementioned processes, does not necessarily lead to a pure cyclostationary process, but leads to an almost cyclostationarity which causes limitation on using cyclostationary features. The authors suggests a new estimator for almost cyclostationary signals.

In most cases, spectrum sensing is based on first order cyclostationary analysis but higher orders can be used to improve the detection probability.

Reference (Giannakis, 1994) defined algorithms to detect presence of cycles in the kth-order cyclic cumulants or polyspectra. Implementation aspects and explicit algorithms for $k < 4$ were discussed. Computationally, algorithms for $k < 3$ are more efficient in the time-domain, while algorithms in the frequency domain are simpler to implement for $k \geq 4$.

Spectrum sensing can be implemented on a single CR device or various CR devices, which collaborate to improve the detection probability. (Lunden, 2009) proposes an energy efficient collaborative cyclostationary spectrum sensing approach for cognitive radio systems, which is also applicable for detecting almost cyclostationary signals where the cyclic period may not be an integer number.

The performance of a detector for OFDM signals based on cyclostationary features is described in (Axell, 2011). The detector exploits the inherent correlation of the OFDM signal incurred by the repetition of data in the cyclic prefix, using knowledge of the length of the cyclic prefix and the length of the OFDM symbol. The authors show that the detection performance improves by 5 dB in relevant cases.

A limited number of papers have described the implementation of spectrum sensing based on cyclostationary analysis. In (Baldini, 2009), the authors present experimental results on the cyclostationarity properties of the IEEE 802.11n Wi-Fi transmissions.

In (Sutton, 2008), the authors describe the implementation of a full OFDM-based transceiver using cyclostationary signatures. The system performance was examined using experimental results.

This book chapter provides the following contributions: we perform experimental analysis to study the performance of detecting Worldwide Interoperability for Microwave Access (WiMAX) 802.16e transmissions through its cyclostationarity features as well as energy detection through the computation of the power spectral density (PSD). The experiment is conducted in an anechoic chamber emulating an Arbritary Waveform Generator (AWG) channel for the communications. We describe the implementation of the demonstrator, which uses cyclostationary signatures on a real CR test platform implemented with Software Defined Radio (SDR) technology. This book chapter describes the main constraints and trade-offs, which influenced the design of the demonstrator. Cyclostationary analysis is computationally intensive and the processing resources of the SDR may be limited for the needed signal processing tasks. We present the results for the estimate of the false alarms and missed detection probabilities for different sets of receiver parameters and for different channel conditions.

This book chapter is organized as follows: in section 2 we present the theoretical background for the cyclostationary spectral analysis followed by the description of the spectrum sensing and detection technique in section 3. In section 4 we present the software defined radio platform used to implement the demonstrator. In section 5, we present the experimental analysis.

2. Cyclostationary signal analysis

A random process $x(t)$ can be classified as wide sense cyclostationary if its mean and autocorrelation are periodic in time with some period T_0. Mathematically they are given by,

$$E_x(t) = \mu(t + mT_0) \tag{1}$$

and

$$R_x(t, \tau) = \pi(t + mT_0, \tau) \tag{2}$$

where, t is the time index, τ is the lag associated with the autocorrelation function and m is an integer. The periodic autocorrelation function can be expressed in terms of the Fourier series given by,

$$R_x(t, \tau) = \sum_{\alpha=-\infty}^{\infty} R_x^{\alpha}(\tau) \exp(2\pi j\alpha t) \tag{3}$$

where,

$$R_x^{\alpha}(\tau) = \lim_{T_0 \to \infty} \frac{1}{T_0} \int_T x(t - \frac{\tau}{2}) x(t + \frac{\tau}{2}) \exp(-2\pi j\alpha t) dt \tag{4}$$

The expression in (4) is known as the cycle autocorrelation, and for a cyclostationary process with a period T_0, the function $R_x^{\alpha}(\tau)$ will have component at $\alpha = 1/T_0$. Using the Wiener relationship, the Cyclic Power Spectrum (CPS) or the spectral correlation function can be defined as,

$$S_x^{\alpha}(f) = \lim_{\tau \to \infty} \int_{-\tau}^{\tau} R_x^{\alpha}(\tau) \exp(-j2\pi f\tau) d\tau \tag{5}$$

The CPS in (5) is a function of the frequency f and the cycle frequency α, and any cyclostationarity features can be detected in the cycle frequency domain. An alternative

expression for (5), for the ease of computing the CPS, is given by,

$$S_x^{\alpha}(f) = \lim_{T\to\infty}\lim_{T_0\to\infty}\frac{1}{T_0 T}\int_{-T/2}^{T/2} X_{T_0}(t, f+\frac{1}{\alpha}) \tilde{X}_{T_0}(t, f-\frac{1}{\alpha})dt \quad (6)$$

where, $\tilde{X}_{T_0}(t,u)$ is the complex conjugate of $X_{T_0}(t,u)$, and $X_{T_0}(t,u)$ is given by,

$$X_{T_0}(t,u) = \int_{t-T_0/2}^{t+T_0/2} x(v)\exp(-2j\pi f v)dv \quad (7)$$

Expression in (6) is also known as the time smoothed CPS which theoretically achieves the true CPS for $T >> T_0$. Figure 1 depicts the CPS of a WiMAX signal generated by means of the theoretical presented in this section. In the following section we present the detector based on the CPS considering the cyclostationarity features of the signal.

3. Energy and cyclostationarity feature based detectors

We use the cyclostationarity feature to detect the presence of WiMAX systems in the radio environment. Based on the sensed noisy signal, the binary hypothesis test to perform the decision is given by,

$$H_0^u : r_u(t) = \nu_u(t); H_1^u : r_u(t) = hs(t) + \nu_u(t), \quad (8)$$

where we have H_0^u when signal is not present and H_1^u when signal is present.

$r_u(t)$ is the signal sensed in the u^{th} frequency cluster, $\nu_u(t)$ is the zero mean band limited Gaussian noise at the receiver front end with a noise power of σ_u^2, and $s(t)$ is the WiMAX signal.

The signal to noise ratio (SNR) can be defined as $SNR = P_s^u/\sigma_u^2$ where P_s^u is the received signal power. We consider the channel h to be slowly varying and hence ignore its statistics in our modeling process below, we also assume that $h \approx 1$ in order to make valid comparisons between different experiments and techniques. Since we use the CPS function to detect WiMAX, we can re-write (8) in terms of the CPS as

$$H_0^u : S_r^{\alpha}(f) = S_{\nu}^{\alpha}(f) H_1^u; S_r^{\alpha}(f) = S_s^{\alpha}(f) + S_{\nu}^{\alpha}(f), \quad (9)$$

where $S_{\nu}^{\alpha}(f)$ is the CPS of the AWGN noise ν, and $S_s^{\alpha}(f)$ is the CPS of the WiMAX signal s. In theory, since ν is not a cyclostationary process, the CPS of ν for $\alpha \neq 0$ is zero. Therefore, by using the CPS, one can detect s when it is present. However, for a finite time duration T, or equivalently a finite length of data in the discrete domain with length $N = T/T_s$, where $f_s = 1/T_s$ is the sampling frequency, noise can be present in $S_r^{\alpha}(f)$ for $\alpha \neq 0$. Based on these arguments, we derive the test statistic for the detector as,

$$Z = \sum_{\alpha}\int_{-f_s/2}^{f_s/2} S_r^{\alpha}(f)\tilde{S}_r^{\alpha}(f)df \quad (10)$$

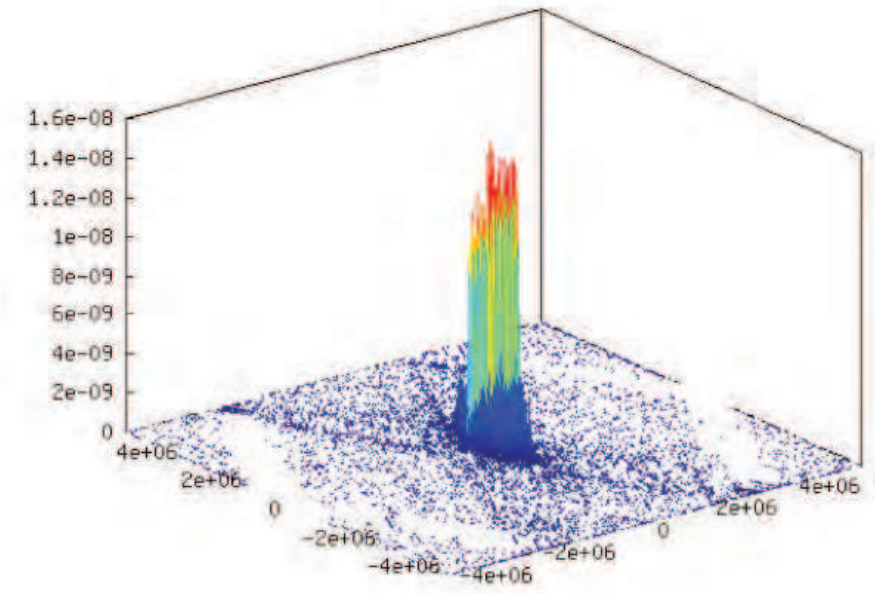

Fig. 1. Cyclostationarity features of a WiMAX signal.

where $\tilde{S}_r^{\alpha}(f)$ is the conjugate of $S_r^{\alpha}(f)$. The detector is then given by,

$$H_0^u : Z < \lambda; H_1^u : Z \geq \lambda$$

where λ is the detection threshold. Finding the optimum threshold is the most crucial aspect of the detector and is generally used to target a particular performance criteria for the false alarm probability and the miss detection probability. In general, knowing the noise variance will allow us to have better threshold values and is also feasible in many practical situations. In our work however, we present the receiver operating characteristic curves for possible values of λ in order to study the detection performance under various conditions and also compare the cyclostationary feature based detection with the classical energy based detection technique, which we present subsequently. For the energy detector (Urkowitz, 1967) based spectrum sensing technique the received signal is passed through an energy detector to compute the test statistics Z which is compared with the threshold λ to make a binary decision on the presence of the WiMAX signal. The test statistic Z for the energy detector are mathematically given by

$$Z = \int_0^T r_u^2(t)dt = T_s \sum_{n=1}^{N} |r_u[n]|^2 \tag{11}$$

where, T is the signal observation time window, T_s is the sampling time of the signal, and N is the total number of samples in time T. Then by using equation (11) we perform the detection process using the threshold λ, which is applied to both energy and cyclostationarity feature based detectors.

4. Software defined radio platform

GNU Software Radio (GSR) is an open source project, which provides a real-time digital signal processing software toolkit to develop SDR and CR applications. It is developed for Linux and usable on many other operating systems (OS) on standard PCs (Gnuradio, 2008). While GSR is hardware-independent, it directly supports the so-called Universal Software Radio Peripheral (USRP) front end designed by Ettus et al. A top-down description of the combined GSR and USRP platform is provided in figure 2. The programming environment

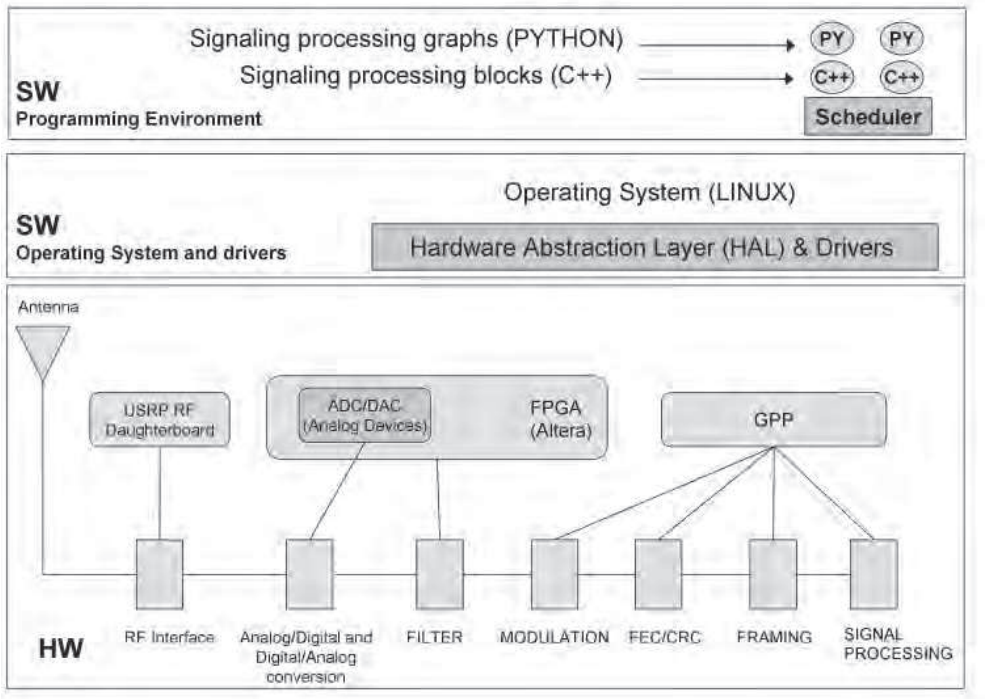

Fig. 2. GNU Radio and USRP architecture

is based on an integrated runtime system composed by a signal-processing graph and signal processing blocks. The signal-processing graph describes the data flow in the SDR platform and is implemented using the object-oriented scripting language Python. Signal processing blocks are functional entities implemented in C++, which operate on streams flowing from a number of input ports to a number of output ports specified per block. Simplified Wrapper and Interface Generator (SWIG) is used to create wrappers for Python around the C++ blocks.

The USRP consists of one main board and up to two receivers (Rx) and two transmitter (Tx) daughterboards. While the main board performs Analog-to-Digital Converter (ADC) and Digital-to-Analog Converter (DAC) conversion, sample rate decimation/interpolation, and interfacing, the daughterboards contain fixed Radio Frequency (RF) front ends including Programmable Gain Amplifiers (PGA) available to adjust the input signal level in order to maximize use of the ADC dynamic range.

This configuration allows an high degree of flexibility because daughter-boards can be connected depending on the type of communications and RF spectrum usage. The ADC/DAC inside the USRP implements sampling and quantization functionality. The analog interface portion contains four ADCs and four DACs. The ADCs operate at 64 million samples per second (Msps) and the DACs operate at 128 Msps. Since the USB bus operates at a maximum rate of 480 million bits per second (Mbps), the Field-Programmable Gate Array (FPGA) must reduce the sample rate in the receive path and it must increase the sample rate in the transmit path to match the sample rates between the high speed data converter and the lower speeds supported by the USB connection. The bottleneck of the system is the USB 2.0 connection to the computer which has, at most, a data rate of 32 MByte/s, thus resulting in a maximum of 8 MS/s of complex signals (16-bit I and 16-bit Q channel).

The ADC/DAC chip is implemented with a AD9862. The AD9862 provides several functions. Each receive section contains four ADCs. Before the ADCs there are PGAs available to adjust the input signal level in order to maximize use of the ADCs dynamic range. The transmit path provides an interpolator and upconverter to match the output sample rate to the DAC sample rate and convert the baseband input to a low IF output. There are PGAs after the DACs. Most of signal processing in the receiver path is performed by the FPGA. The standard FPGA

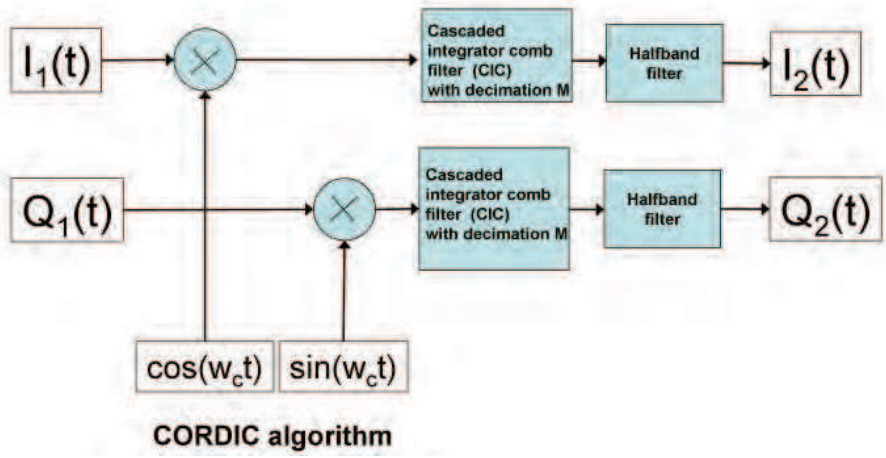

Fig. 3. Block diagram of the digital down-conversion and decimation stage

firmware provides two Digital Down Converters (DDC). The FPGA uses a multiplexer to connect the input streams from each of the ADC's to the inputs of the DDC's. This multiplexer allows the USRP to support both real and complex input signals. The DDC operate as *real* down converters using the data from one ADC fed into the real channel or as *complex* DDCs where the data from one ADC is fed to the real channel and the data from another ADC is fed to the complex channel via the multiplexer.

Figure 3 provides a description of the digital down-conversion and decimation stage to generate the down-converted signal I_2+jQ_2 from the received I_1+jQ_1. W_c represents the frequency for the down-conversion based on the local oscillator, M is the decimation parameter in the Cascaded Integrator Comb (CIC) filter . M is an important parameter for the trade-offs described in the following paragraphs. USRP uses the CORDIC algorithm in the down-conversion (see (Vankka, 2000) for a description of the CORDIC algorithm).

5. Experimentation

5.1 Test setup

This section describes the test-bed setup used for the detection and analysis of the Worldwide Interoperability for Microwave Access (WiMAX) signal. The test-bed setup is described in figure 4. The main components of the test-bed are:

- model RSA3408 spectrum analyzer by Tektronix. It has a frequency range from DC to 8 GHz, 36 MHz bandwidth and a very low background noise floor (-150 dBm/Hz at 2 GHz and a frequency range).
- Rohde & Schwarz SMBV100A signal generator to generate the WiMAX signal based on different standards (e.g. 802.16d and 802.16e). The signal generator has a frequency range from 9 kHz to 6 GHz and very low SSB phase noise (less than -122 dBc at 1 GHz).
- USRP platform already described in section 4.
- variable attenuator with range 0-81 dB to simulate different distances between the WiMAX signal generator and the receiver (i.e. USRP platform).

The signal generator is connected to the receivers (i.e. spectrum analyzer and the USRP platform) through low-loss cables (i.e. 0.327 dB of attenuation at 3.63 GHz). The variable attenuator is needed to simulate various distances between the signal generator and the receivers and to validate the efficiency of the detection algorithm based on cyclostationary features. Signal detection through cyclostationary features is particularly efficient in comparison to signal detection through power sensing when the received signal is at level of the noise floor or below the noise floor. Measurements were repeated with increasing levels of attenuation to validate the signal detection algorithm. Experiments were conducted by generating the WiMAX signal with the features shown in table 1.

Modulation scheme	OFDM
Standard version	802.16 2004-2005
Burst Type	FCH
Modulation	16QAM
Frame	ETSI
Burst length	*3 ms*

Table 1. Features of the WiMAX signal.

5.2 Implementation of the detectors

As described in section 4, the limitation of USB 2.0 to 8 MS/s can increase the spectrum scanning time for a wide frequency band (e.g. 100 MHz). The spectrum scan is implemented by dividing the spectrum in portions of maximum 8 MHz. The algorithm works like a Sliding Spectral Window Technique to cover the entire desired radio frequency spectrum. The algorithm scans the radio frequency spectrum of interest, collecting and processing the data. The same algorithm is used both for *energy detector* based sensing and for *cyclostationary detector* based sensing.

The block diagram for the *energy detector* unit is presented in figure 5. The block diagram for the *cyclostationary detector* is presented in figure 6. Each of the blocks represents a specific signal processing stage programmed in C++. The blocks, which are identified as "Variable",

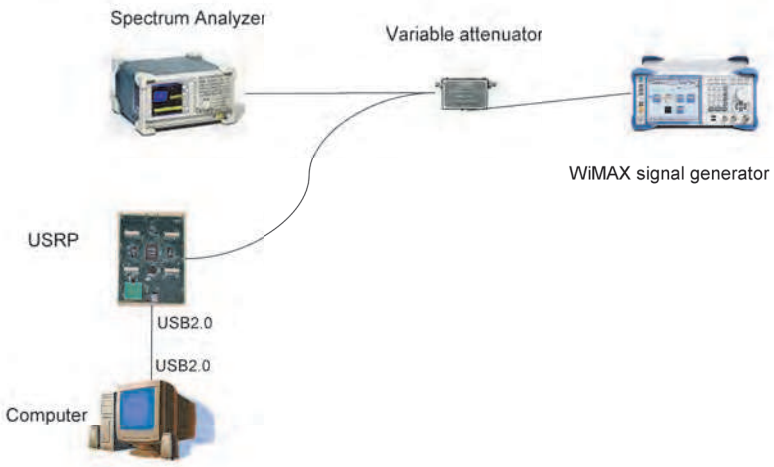

Fig. 4. Test bed configuration

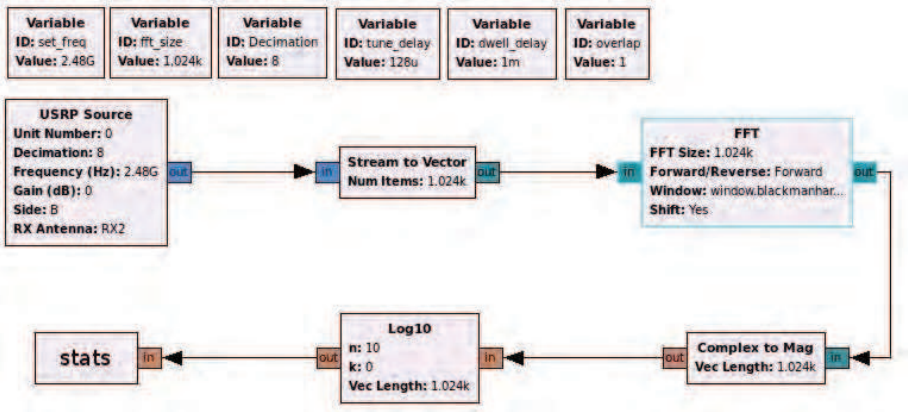

Fig. 5. Block diagrams of the power spectrum algorithm implemented in the *GNU Radio* to calculate the PSD

allow us to dynamically modify the system variables and they will be further discussed in section 5.3.

The first block *USRP source* implements the tuning functionality to tune the receiver to a specific frequency with a bandwidth defined by the decimation value, which is chosen to optimize the processing of the received radio signal. For example, by choosing the maximum decimation value (i.e. 8), we will have a bandwidth of 8 MHz and a sampling frequency of 8

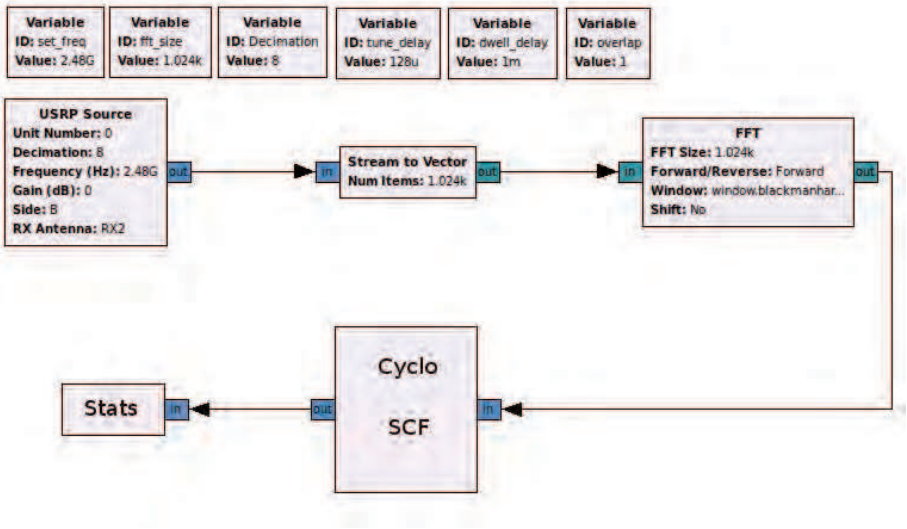

Fig. 6. Block diagrams of the cyclostationary algorithm implemented in the *GNU Radio* to calculate the PSD

MS/s. The received signal is then converted and sampled by the USRP and processed by the *Stream to Vector* block to convert the complex data flow to a complex vector flow. The signal is then multiplied for a window of Blackman-Harris type, to improve the efficiency of the overall algorithm, and then brought in the frequency domain by Fast Fourier Transform (FFT). At this point, the flow diagrams are different for the *energy detector* and the *cyclostationary detector*. In the *energy detector* the *Complex to Mag* block calculates the signal magnitude, which is logarithmic converted by the Log_{10} block and converted to the the Power Spectral Density (PSD). As described in section 3, by choosing an appropriate threshold, it is possible to detect, in real time, the presence/absence of the communication signal. The threshold are computed empirically by calibrating the receiver on continuous wave signals, with defined power levels, transmitted by a signal generator.

In the *cyclostationary detector* flow, the *Cyclo SCF* block calculates the Spectral Correlation Function (SCF) for all of the values of cyclic frequency and the Z on the basis of the theoretical framework described in section 3. By choosing the optimum threshold, the cyclostationary components of the signal can be identified.

Finally, in both flows, the *Stats* block is responsible for the management of the "spectrum scanning" functionality. Specifically, it is responsible for the USRP tuning and the sampling of the received data to be analyzed or discarded.

The real time estimation has a trade-off between the smaller resolution request to estimate the SCF and the USRP's bandwidth. Therefore decimation and length of the FFT are two parameters, which can be used to improve the performance of both detectors. This choice defines the length of processing time: in the case of the energy detector it is proportional to the decimation and to the number of samples on which FFT is calculated; instead for the cyclostationary detector it is proportional to the decimation and to the square number of samples on which FFT is calculated.

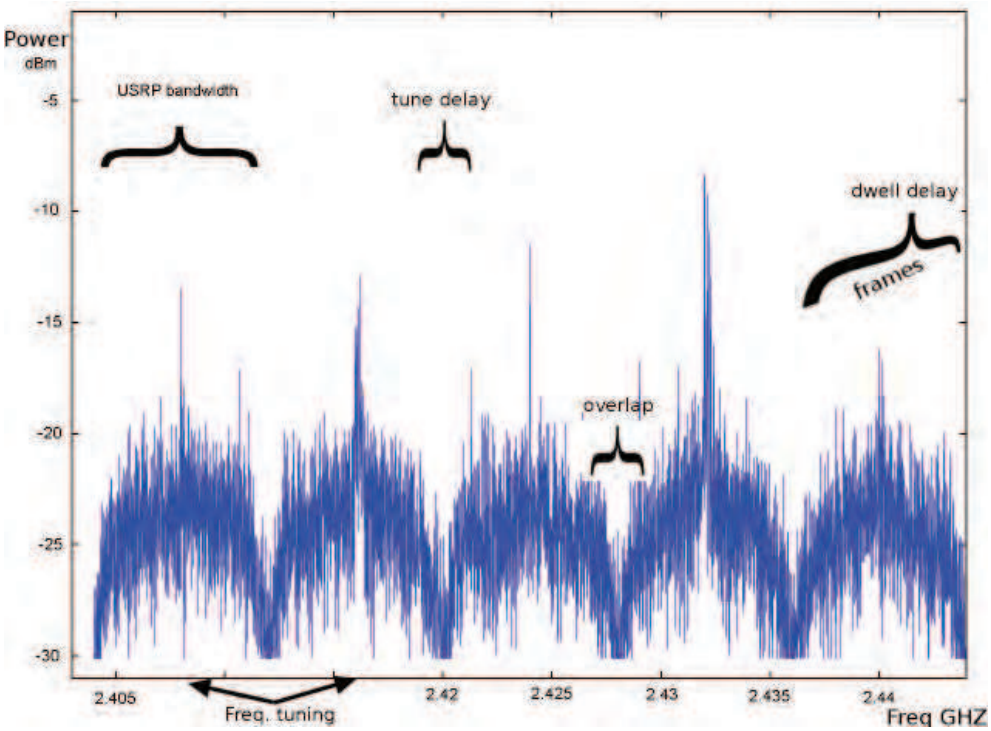

Fig. 7. Spectrum scanning of a band of 40 MHz by using windows of 8 MHz each

5.3 Sensing parameters and related trade-offs

The selection of sensing parameters is an important element to improve the sensing algorithm. The sensing time represents a major trade-off: the increase of the sensing time will reduce the probability of false alarms, but it will also increase the overall the time for scanning the radio frequency spectrum.

To detect the presence of a pulse signal of a short time duration (i.e. burst), we have to scan the spectrum as swiftly as possible. The scanning is carried out by sliding the USRP's Radio Frequency (RF) front-end in shifted frequency given by the relation between the fixed sampling rate of the USRP's ADC/DAC (64 MSa/s) and the decimation choice. Our purpose is to find the best combination between these parameters to improve the probability of detection and to keep the sensing time the shortest possible in order to operate the cyclostationary detection algorithm in real time on the USRP platform. In this book chapter, we will use the experimental results to support the choice of the parameters.

In figure 7, we describe the spectrum scanning concept for a band of 40 MHz and we identify the most important parameters, which contribute to the performance of the spectrum scanning.

The combination of the parameters identified in figure 7 and figures 5 and 6 (i.e. implementation of the detection algorithms) define the overall set of parameters, which drive the performance of the SDR receiver:

1. The ***tuning frequency***: the selection of the center band frequency where the USRP operates;
2. The ***decimation*** (M): define the bandwidth of the RF front-end of the USRP, the sampling frequency on the basis of the following definition:

$$USRP_{rate} = \frac{ADCrate}{M} \tag{12}$$

3. the ***fft size*** where (NFFT) is the number of sampling on which FFT is calculated;
4. the ***tune delay*** (*Td*) is the needed time for the RF front-end to synchronize to a specific frequency. The USRP has a limited throughput so a number of samples must be eliminated on the basis of the following formula:

$$N_{Td} = \frac{Td \cdot USRP_{rate}}{NFFT} \tag{13}$$

5. The ***dwell delay*** (*Dd*) is the time where USRP is synchronized to a specific frequency (i.e. signal observation time).

$$N_{Dd} = \frac{Dd \cdot USRP_{rate}}{NFFT} \tag{14}$$

6. The ***overlap*** is the overlapping of two consecutive spectral windows; it is expressed as a fraction. A value of 100% means that there is no overlapping.

In order to improve the probability of detection and to optimize the sensing time for real-time operation the choices of these parameters are essential.

To serve such purpose we will conduct an analysis of the parameters identified above on the basis of experimental tests. The first consideration is based on the general assumption of the absence of a receiver filter. As described in Section 4, the USRP is not equipped with a receiver filter and additional signal processing techniques are needed for the filtering function. The *overlap* parameter is used to address the absence of the receiver filter in the USRP. The *overlap* works like a band pass filtering centered to the USRP's frequency tuning. The trade-off of the *overlap* parameter is a better filtering and suppression of signal repetitions at the cost of loss of samples, during the acquisition process. For example, if the *overlap* is selected to a value of 0.75, 25% of the data received for every window may be discarded, while the frequency distance between two adjacent windows will be reduced by 25%, reducing the risk of signal's repetitions in the adjacent bands in which the signal is sensed.

The *Td* is the time to manage the incoming data between two adjacent frequency windows. USRP has the limitation that it is not possible to block the flow graph, while it is processing the received data. The processing time and the sampling rate should be synchronized. This is not always possible with complex signals like WiMAX. Before processing the data at the frequency at which the RF front-end is tuned in, the USRP may discard the received data from the previous frequency window still present in the USB pipeline. A reasonable short time to minimize the discarded data is chosen to be equal to *10 ms*, which for *M* equal to 8 and *NFFT* equal to 1024 results in 78 records discarded at each frequency change. On the basis of these considerations, we decided to define the *Td* and the *overlap* constant for all the measurements, and equal respectively to *10 ms* and to *0.75*.

The *Dd* or dwell delay is the signal observation time for each frequency window the RF front-end is tuned in. It is selected based on the hardware elaboration speed. It depends

*NFFT**M*	128	256	512	1024	2048	Units
8			3906,25 39 64	7812,5 78 128	15625 156 256	r in Hz S_s in ♯ T_p in ms
16		3906,25 39 64	7812,5 78 128	15625 156 256		r in Hz S_s in ♯ T_p in ms
32	3906,25 39 64	7812,5 78 128	15625 156 256			r in Hz S_s in ♯ T_p in ms

Table 2. Frequency resolution (r), number of records discarded (S_s) and elaboration time (T_p) needed for a single window reference to M and $NFFT$.

upon the choice of the value of decimation: for M equal to 8, the time to collect 1024 samples is equal to 128 ms.

As illustrated in table 2, the decimation and number of samples on which FFT is calculated determines the value of:

- frequency resolution: r in Hz.
- number of records discarded for each frequency change: S_s in ♯.
- minimum hardware time needed to process data from a single window: T_p in ms.

In order to examine the performance of the receiver implementation outlined in the previous section, we executed measurement campaigns with the WiMAX parameters defined in table 1.

Figure 8 shows a spectrum scanning from 2.4 GHz to 2.5 GHz using the Energy Detector for 35 seconds of sensing time. The frequency peak at 2.405 GHz represents a WLAN signal, which was present in the measurement environment but it not part of the experiment. The WLAN signal was filtered out in the signal analysis phase. The WiMAX signal generated with 0 dBm power appears at 2.484 GHz. Figure 9 describes the SCF estimates for the same experiment. The SCF is presented at the central frequency of 2.484 GHz for a bandwidth of 4 MHz and using a 256-bin Fourier transform. From the figure we clearly identify all the WiMAX signal sub-carriers at the cycle frequencies $\alpha = 4MHz$.

We have generated WiMAX signal with an increasing number of channels (from 1 to 8). Examples of the resulting SCFs are shown in figure 10 (two channels) and figure 11 (eight channels).

5.3.1 Detection performance in relation to FFT-bin size and decimation

A number of tests were executed with changing values of the USRP's decimation, bandwidth and FFT-bin size, to investigate the performance of the detector. From section 3, we can obtain the equations for the percentages of false alarm and detections, which are given by:

$$\begin{aligned} P_{FA} &= P(Z > \lambda | H0) \\ P_D &= P(Z > \lambda | H1) \end{aligned} \tag{15}$$

By using the AWGN source generator, we set the threshold to reach the percentage of false alarm, P_{FA}, of 10^{-3}. The WiMAX signal is transmitted at a range of power levels, centered at 2.484 GHz. In the test, we used a signal observation time equal to *1,28 ms*. For every

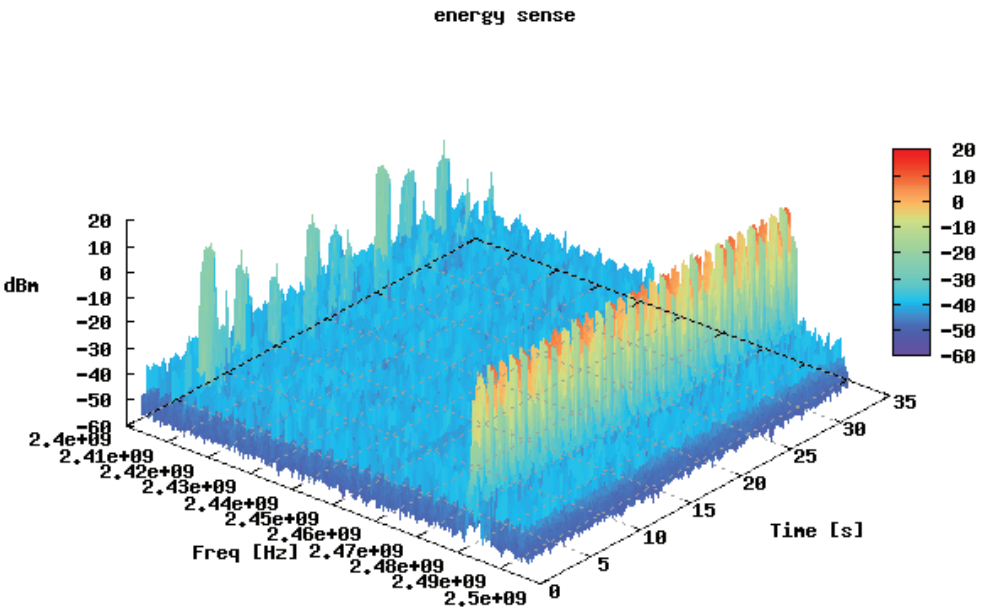

Fig. 8. PSD for *35 s* of spectrum sensing from 2,4 GHz to 2,5 GHz; WiMAX signal

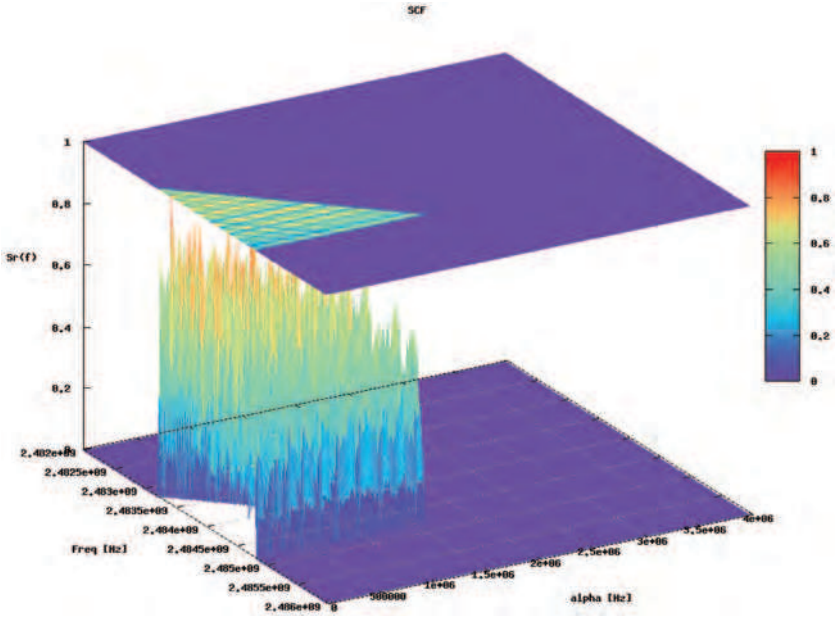

Fig. 9. SCF at the frequency of 2,484 GHz; WiMAX signal, which uses all the available channels

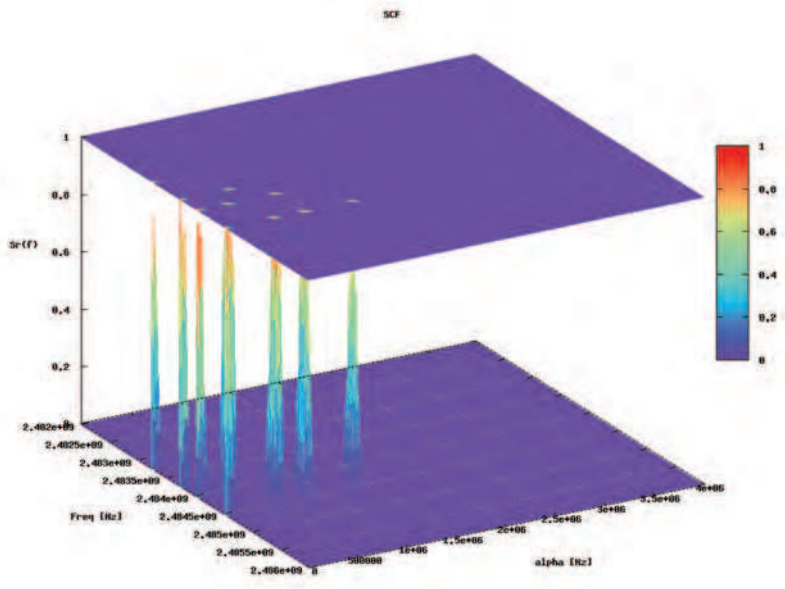

Fig. 10. SCF at the frequency of 2,484 GHz; WiMAX signal, which uses only two channels.

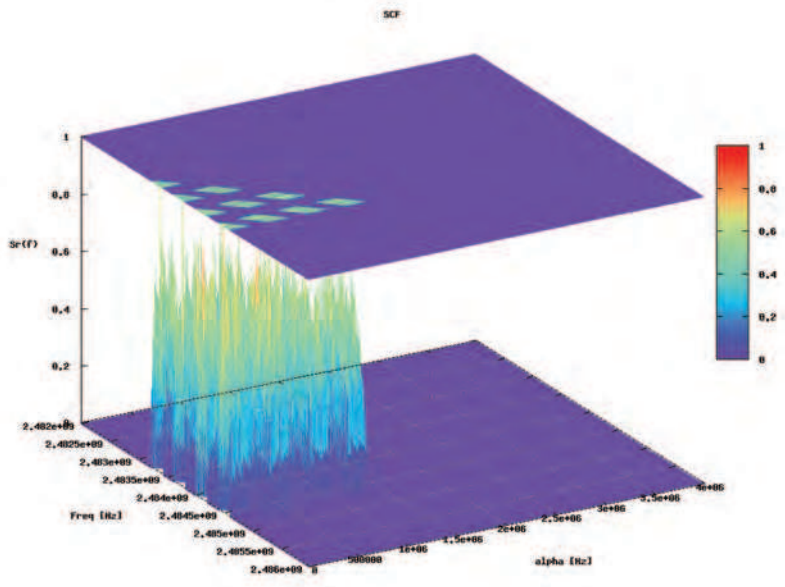

Fig. 11. SCF at the frequency of 2,484 GHz; WiMAX signal, which uses only eight channels.

combination of *NFFT* and *M*, the percentage of detection is estimated. The results are illustrated in figures 12 and 13 respectively for *energy detector* and for the *cyclostationary detector*. For both detection techniques the performances improved using the smallest USRP's bandwidth. This is caused by the inability of the processor to manage the incoming data from the USRP. This effect is greater in the *cyclostationary detector* than the *energy detector* due to the higher complexity of the cyclostationary detection algorithm. The best detection performance is for values of decimation set to 32 and FFT-bin size to 128.

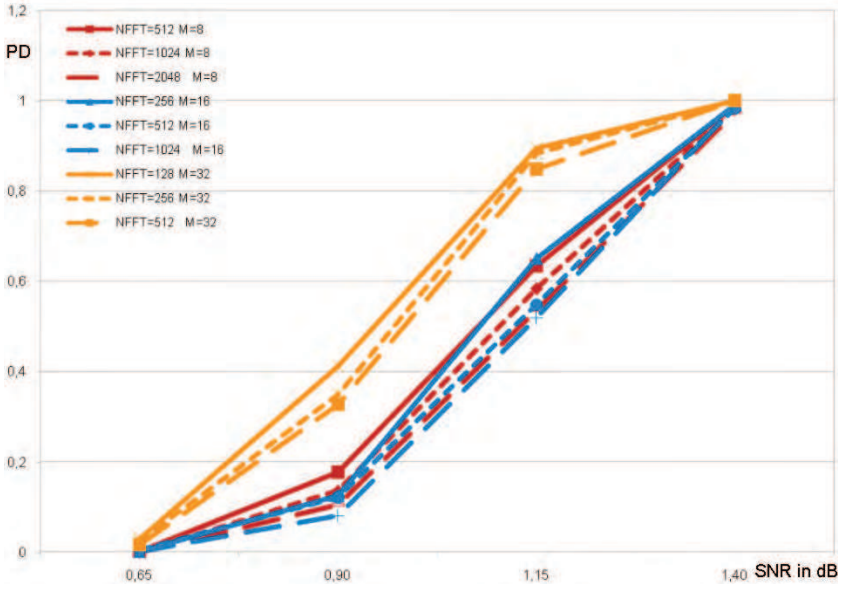

Fig. 12. PD for the power detection technique in relation to Signal/Noise ratio for combinations of NFFT and M.

5.3.2 Detection performance in relation to observation time

Ten thousands tests were executed to examine the performance for both detectors with increasing signal observation time *Td*. Naturally, this value must be chosen in relation to the requested speed of the spectrum scanning and the type of signal to be detected (e.g. WiMAX). Using a pulse signal type the observation time have to be lower than the duration of the single burst. Using an AWGN source generator we set the threshold to reach the percentage of false alarm, P_{FA}, of 10^{-3}. WiMAX signal is transmitted at a range of power levels, centered at 2.484 GHz. Figure 14 describes the percentage of detection for received SNR. Performance is seen to improve considerably with increased observation time from 0.064 ms to 0.36 ms for both detection techniques.

Table 3 displays the processing times required to scan 100 MHz of spectrum for *energy detector* (PSD) and *cyclostationary detector* (SCF). The energy detector algorithm spends *0.36 ms* for every combination of *NFFT* and *M*. Real time elaboration is possible only if the time spaces between the signal bursts are shorter than *3,6 ms*. As expected the *cyclostationary detector* has longer processing times and for some combinations of *NFFT* and *M*, real time elaboration is not possible.

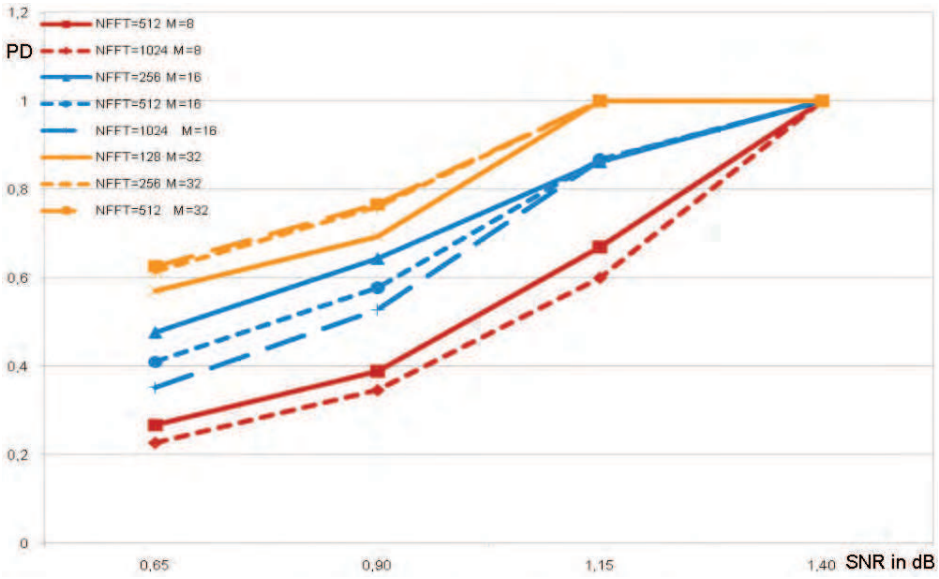

Fig. 13. PD for the cyclostationarity detection technique in relation to Signal/Noise ratio for combinations of NFFT and M.

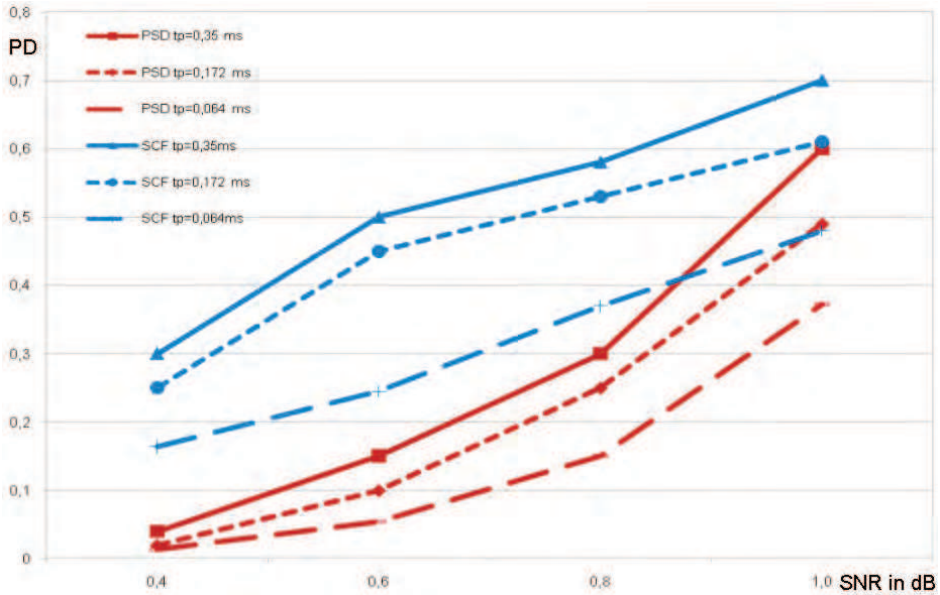

Fig. 14. Time Performance, percentage of detection PD for both detection techniques increasing observation time.

NFFT\M	128	256	512	1024	2048	Detector
8			0.35	0.36	0.39	$T_p(PSD)$
			3.12	11.69	44.32	$T_p(SCF)$
16		0.37	0.36	0.38		$T_p(PSD)$
		1.5	6.08	22.68		$T_p(SCF)$
32	0.36	0.37	0.38			$T_p(PSD)$
	0.84	3.13	11.04			$T_p(SCF)$

Table 3. Time Performance, processing times (T_p) required to scan 100 MHz of spectrum.

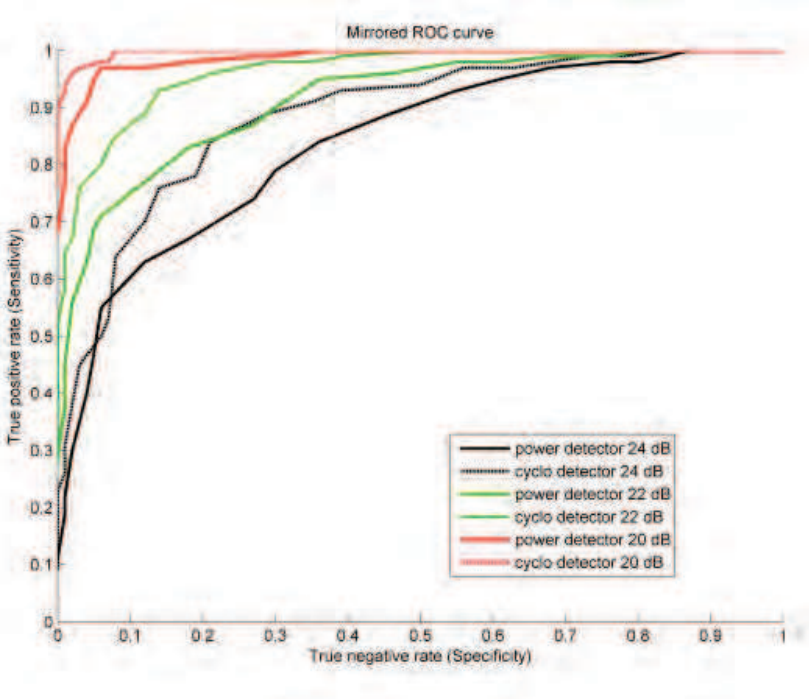

Fig. 15. Receiver operation characteristic (ROC) performance for various SNR levels, energy based detector against cyclostationary based detector.

5.3.3 Receiver operating characteristic (ROC)

Figure 15 describes the receiver operating characteristic (ROC) curves for ten thousand measurements performed for both detectors for various SNR levels. The signal is received using USRP, which was configured to process a spectrum band of 2 MHz bandwidth centered to 2.484 GHz. The experimental results show a significant increase in gain in the curves with increased SNR. The figure 15 also shows that the cyclostationary based detector perform better than the energy based detector in discriminating against the additive sensing noise. This confirms the robustness of the cyclostationary detection algorithm with low SNR in comparison to the energy detector. The trade-off is that cyclostationary detection is computationally more complex and requires significantly longer signal observation time to get a precise estimate of SCF to perform the detection.

6. Conclusion and future developments

This book chapter presents an experimental evaluation of the cyclostationary and energy based spectrum sensing techniques for cognitive radios, implemented on a functional software defined radio platform. The sensing techniques were tested against a WiMAX signal generated in an anechoic chamber emulating an AWGN communications channel. The parameters that affect the real-time detection performance of the cognitive radios were evaluated. Moreover, we presented the trade-offs among the main parameters (e.g. FFT size, decimation) in relation to different values of SNR and observation time. Our results show that the cyclostationarity based technique performs well in comparison to the energy based detector at the expense of additional computational complexity. In particular, the cyclostationary based technique requires more time samples to generate the cyclic spectral density with the needed level of accuracy.

Our future developments will include the design and implementation of an adaptive sensing algorithm, which can tune automatically to the described parameters as well as selecting the best detection techniques for any wireless communication systems (i.e. not only WiMAX) in any radio environment. The adaptive scanning approach will thus require more sophisticated and efficient cyclostationary detection methods. The authors will investigate and apply other computationally efficient algorithms such as the Strip Spectral Correlation Algorithm (SSCA) described in (Roberts, 1991).

7. References

FCC, Spectrum Policy Task Force Report, ET Docket No. 02-155, Nov 02, 2002.

FCC White Spaces Access Rules: "Unlicensed Operation in the TV Broadcast Bands", Final Rules (http://edocket.access.gpo.gov/2009/pdf/E9-3279.pdf). Last Accessed 10 September 2010.

J. Mitola and G. Maguire Jr., Cognitive Radio: Making Software Radios More Personal, *IEEE Personal Communications*, vol. 6, no. 4, pp. 13 8, Aug. 1999.

S. Haykin, Cognitive Radio: Brain-Empowered Wireless Communications, *IEEE Journal on Select Areas in Communications*, vol. 23, no. 2, pp. 201 - 220, Feb. 2005.

Ed Arslan, Cognitive Radio, Software Defined Radio, and Adaptive Wireless Systems, Springer, Netherlands, 2007.

V. Bhargava, Cognitive Wireless Communication Networks, Springer, New York, 2007.

Federal Communications Commission, Facilitating Opportunities for Flexible, Efficient, and Reliable Spectrum Use Employing Cognitive Radio Technologies, NPRM and Order, ET Docket no. 03-322, Dec. 2003.

The Commission of the European Communities, Commission Decision 2007/131/EC on allowing the use of the radio spectrum for equipment using ultra-wideband technology in a harmonised manner in the Community, Official Journal of the European Union, Feb. 21, 2007.

W.A. Gardner, Exploitation of spectral redundancy in cyclostationary signals, *IEEE Signal Processing Magazine*, Vol 8,April 1991,pp 14-36.

W. A. Gardner and L. E. Franks, ŞCharacterization of cyclostationary random processes,Ť *IEEE Trans. Inform. Theory*, vol. 21, pp. 414, 1975.

R.S. Roberts, W.A. Brown, H.H. Loomis, Computationally efficient algorithms for cyclic spectral analysis, *IEEE Signal Processing Magazine*, April 1991, Vol 8, Iss 2, pp 38-49.

S. Kandeepan; G. Baldini; R. Piesiewicz; , Experimentally detecting IEEE 802.11n Wi-Fi based on cyclostationarity features for ultra-wide band cognitive radios, *Proceedings*

of the 2009 IEEE 20th International Symposium on Personal, Indoor and Mobile Radio Communications, vol., no., pp.2315-2319, 13-16 Sept. 2009.

A. Tkachenko, A.D. Cabric, R.W Brodersen, Cyclostationary Feature Detector Experiments Using Reconfigurable BEE2, *Proceedings of the 2007 IEEE International Symposium on New Frontiers in Dynamic Spectrum Access Networks (DySPAN)*, 17-20 April 2007, pp 216-219, Dublin.

Kyouwoong Kim Akbar, I.A. Bae, K.K. Jung-sun Urn Spooner, C.M. Reed, J.H., Cyclostationary Approaches to Signal Detection and Classification in Cognitive Radio, *Proceedings of the 2007 IEEE International Symposium on New Frontiers in Dynamic Spectrum Access Networks (DySPAN)*, 17-20 April 2007 pp 212-215, Dublin.

S. Enserink, D. Cochran, "A cyclostationary feature detector", *Proceedings of the Twenty-Eighth Asilomar Conference on Signals, Systems and Computers*, 31 Oct-2 Nov 1994 Vol 2, pp806-810, Pacific Grove, CA.

M. Oner; F. Jondral, "Cyclostationarity based air interface recognition for software radio systems", *Proceedings of the IEEE Radio and Wireless Conference*, 19-22 Sep. 2004 pp 263-266.

Eric Blossom, Exploring GNU Radio. http://www.gnu.org/software/gnuradio/doc/exploring-gnuradio.html. Last Accessed 16 September 2008.

H. Urkowitz, Energy Based Detection of Unknown Deterministic Signals, *IEEE Proceedings*, Vol.55, No.4, page:523-531, April 1967.

T. Yucek; H. Arslan; "A survey of spectrum sensing algorithms for cognitive radio applications," *IEEE Communications Surveys & Tutorials*, vol.11, no.1, pp.116-130, First Quarter 2009

J. Vankka; M. Kosunen; I. Sanchis; K.A.I. Halonen; "A multicarrier QAM modulator," *Circuits and Systems II: IEEE Transactions on Analog and Digital Signal Processing*, vol.47, no.1, pp.1-10, Jan 2000

A. V. Dandawatk and G. B. Giannakis, "Statistical Tests for Presence of Cyclostationarity", *IEEE Transactions on signal processing*, vol. 42, no. 9, September 1994.

Hosseini, S.M.A.T.; Amindavar, H.; Ritcey, J.A.; , "A new cyclostationary spectrum sensing approach in cognitive radio," *Proceedings of the 2010 IEEE Eleventh International Workshop on Signal Processing Advances in Wireless Communications (SPAWC)*, vol., no., pp 1-4, 20-23 June 2010.

Lunden, J.; Koivunen, V.; Huttunen, A.; Poor, H.V.; , "Collaborative Cyclostationary Spectrum Sensing for Cognitive Radio Systems," *IEEE Transactions on Signal Processing*, vol.57, no.11, pp 4182-4195, Nov. 2009.

Sutton, P.D.; Nolan, K.E.; Doyle, L.E.; , "Cyclostationary Signatures in Practical Cognitive Radio Applications," *IEEE Journal on Selected Areas in Communications*,vol.26, no.1, pp 13-24, Jan. 2008.

Axell, E.; Larsson, E.G.; , "Optimal and Sub-Optimal Spectrum Sensing of OFDM Signals in Known and Unknown Noise Variance," *IEEE Journal on Selected Areas in Communications*, vol.29, no.2, pp.290-304, February 2011

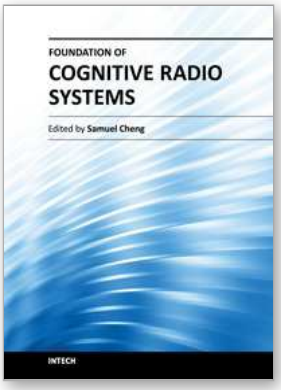

Foundation of Cognitive Radio Systems

Edited by Prof. Samuel Cheng

ISBN 978-953-51-0268-7
Hard cover, 298 pages
Publisher InTech
Published online 16, March, 2012
Published in print edition March, 2012

The fast user growth in wireless communications has created significant demands for new wireless services in both the licensed and unlicensed frequency spectra. Since many spectra are not fully utilized most of the time, cognitive radio, as a form of spectrum reuse, can be an effective means to significantly boost communications resources. Since its introduction in late last century, cognitive radio has attracted wide attention from academics to industry. Despite the efforts from the research community, there are still many issues of applying it in practice. This books is an attempt to cover some of the open issues across the area and introduce some insight to many of the problems. It contains thirteen chapters written by experts across the globe covering topics including spectrum sensing fundamental, cooperative sensing, spectrum management, and interaction among users.

How to reference

In order to correctly reference this scholarly work, feel free to copy and paste the following:

Gianmarco Baldini, Raimondo Giuliani, Diego Capriglione and Kandeepan Sithamparanathan (2012). A Practical Demonstration of Spectrum Sensing for WiMAX Based on Cyclostationary Features, Foundation of Cognitive Radio Systems, Prof. Samuel Cheng (Ed.), ISBN: 978-953-51-0268-7, InTech, Available from: http://www.intechopen.com/books/foundation-of-cognitive-radio-systems/a-practical-demonstration-of-spectrum-sensing-for-wimax-based-on-cyclostationary-features

INTECH
open science | open minds

InTech Europe
University Campus STeP Ri
Slavka Krautzeka 83/A
51000 Rijeka, Croatia
Phone: +385 (51) 770 447
Fax: +385 (51) 686 166
www.intechopen.com

InTech China
Unit 405, Office Block, Hotel Equatorial Shanghai
No.65, Yan An Road (West), Shanghai, 200040, China
中国上海市延安西路65号上海国际贵都大饭店办公楼405单元
Phone: +86-21-62489820
Fax: +86-21-62489821

© 2012 The Author(s). Licensee IntechOpen. This is an open access article distributed under the terms of the Creative Commons Attribution 3.0 License, which permits unrestricted use, distribution, and reproduction in any medium, provided the original work is properly cited.